

# Active Sites of Cu/ZnO-Based Catalysts for CO<sub>2</sub> Hydrogenation to Methanol: Part II

## Reaction mechanisms, bulk structure and multiscale modelling

### Mustafa Al Salmi\*

Petroleum Development Oman, PO Box 81,  
Muscat, Oman

Email: \*Mustafa.MMA.Alsalmi@pdo.co.om

### PEER REVIEWED

Received 15th December 2023; Revised 10th March 2024; Accepted 14th March 2024; Online 14th March 2024

Part II of this review continues to explore the connection between Cu/ZnO-based catalysts properties and methanol synthesis activity. This work continues from Part I (1).

### Keywords

Cu/ZnO catalysts, CO<sub>2</sub> hydrogenation, methanol, active sites, structure characterisation

## 1. Reaction Mechanism of CO<sub>2</sub> Conversion into Methanol through Formate Pathway

HCOO is the key intermediate for CO<sub>2</sub> hydrogenation to methanol from syngas (hydrogen, CO<sub>2</sub> and carbon monoxide) as the formate species is formed from CO<sub>2</sub> and hydrogen (2–4). It was found that formation of formate species takes place on the ZnO/Cu(111) surface (5) and it is the most active intermediate in this pathway as it has a low energy barrier. The reverse reaction that forms the formic acid intermediate is not stable, meaning it decomposes back to formate and because of this, strongly bound formate species occupy the surface

site. However, the strong binding of formate and methoxide with the surface can poison the Cu/ZnO catalyst and as a result, the production of methanol decreases over time (5). In general, the production of methanol is hindered by H<sub>3</sub>CO hydrogenation to methanol, although the accumulation of \*H<sub>3</sub>CO is not as much as that of formate. Furthermore, Li *et al.* reported that the catalytically active copper sites are mainly located in the interface between metallic copper and the zinc oxide substrate, which results in a synergetic interaction taking place between copper and zinc oxide (5). In addition, they found that hydrogenation of CO<sub>2</sub> on the Cu/ZnO catalyst takes place on the Cu<sup>+</sup> sites with the formation of the HCOO intermediate bridged on two copper atoms (5). Furthermore, it was found that two adsorbed hydrogen atoms attach to the adsorbed formate to form dioxomethylene (H<sub>2</sub>COO) species, then decompose into formaldehyde (H<sub>2</sub>CO) and hydroxyl (OH). The H<sub>2</sub>CO species then reacts with two hydrogen atoms to form methoxy (CH<sub>3</sub>O) species and methanol (see Figure 1 in Part I (1)) (2, 5–7).

On the other hand, Yang *et al.* concluded that the presences of low-coordinated active sites on copper nanoparticles leads to enhanced catalytic activity of CO<sub>2</sub> hydrogenation to methanol (8). Therefore, the highly active and selective catalysts for CO<sub>2</sub> to methanol conversion *via* the formate pathway should contain Cu and Cu<sup>+</sup> sites, which lower the energy barriers for H<sub>2</sub>COO and HCOO. Grabow and Mavrikakis, in 2011, reported that the activation barriers for the hydrogenation of HCOO species to HCOOH is about –0.20 eV, which is lower than the activation barrier for HCOO to H<sub>2</sub>COO, which is –0.90 eV (5, 9). In addition, they observed that HCOOH was the major product due

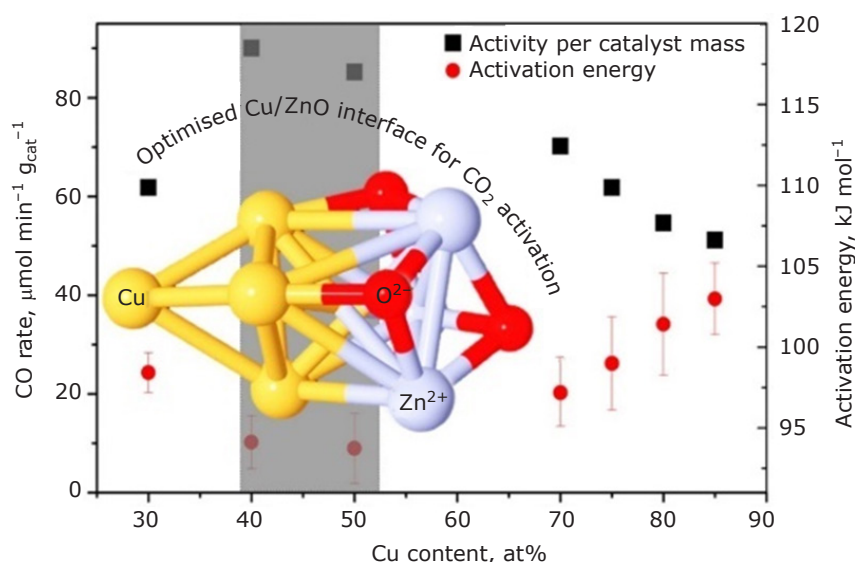


Fig. 1. The relationship between the carbon monoxide rate and activation energy of an optimised Cu–ZnO interface for CO<sub>2</sub> activation (47). Copyright 2016 Elsevier

to the hydrogenation of the HCOO intermediate. The HCOOH was then hydrogenated to H<sub>2</sub>COOH species and then to H<sub>2</sub>COO in a mechanism known as the revised HCOO (r-HCOO) mechanism (8). In addition to this, Grabow and Mavrikakis reported that the dissociation of CH<sub>3</sub>O<sub>2</sub> to formaldehyde is desirable over the H<sub>2</sub>COO dissociation. Therefore, they concluded that r-HCOO is more likely to take place on Cu(111) (9).

Within the formate pathway for CO<sub>2</sub> conversion to methanol, the reversed (r-HCOO) mechanism has emerged as a potential contender for the dominant reaction pathway. Here, formate (HCOO\*) acts as a key intermediate. Behrens *et al.* investigated the role of zinc doping on Cu(211) surfaces using theoretical calculations (10). Their findings highlight the importance of zinc doping in promoting the r-HCOO mechanism. Zinc doping enhances the stability of surface oxygen-bound intermediates, such as CH<sub>3</sub>O\*, which are crucial steps in the r-HCOO pathway. This translates to lower energy barriers, making the overall conversion of CO<sub>2</sub> to methanol more efficient. Behrens *et al.* further observed that stepped zinc-free and zinc-doped sites exhibit increased activity for methanol formation through the r-HCOO mechanism. Based on their findings, Behrens *et al.* concluded that the r-HCOO mechanism might be more favourable compared to the traditional HCOO mechanism for methanol production.

Understanding the bonding configuration of formate on the copper surface is crucial for elucidating the reaction mechanism. Several studies have explored the bonding modes of formate on copper surfaces using various techniques. Density

functional theory (DFT) calculations offer valuable insights into these configurations. Chutia *et al.* (11) investigated different formate adsorption models on copper surfaces using DFT calculations. Their calculations revealed that after relaxation, initially proposed monodentate and bidentate configurations with one or two oxygen atoms bonded to the same copper atom, respectively, transformed into bidentate configurations with both oxygen atoms bonded to separate copper atoms on the surface (12). This bidentate configuration exhibited a significantly lower adsorption energy compared to other models, suggesting a more stable bonding arrangement. This indicates a stronger interaction and potentially higher stability for this specific bidentate configuration. Additionally, they determined that the bidentate formate molecule adopts a near-perpendicular geometry (~88°) relative to the copper surface (11).

Further to this, the geometrical and electronic structure of the formate species on the Cu(110), Cu(111) and Cu(100) crystallographic planes was studied using different exchange and correlation functionals such as PW91, PBE, PBE-D2 and PBEsol. Atodiresei *et al.* (13) and Hu *et al.* (14) also reported the geometrical and electronic properties of the formate species on Cu(110). They found a bridge configuration along the (1 $\bar{1}$ 0) plane, with oxygen atoms on top of the copper atoms. In addition, it was found that formate species adopted a perpendicular position on the Cu(110) surface (15). Additionally, they found that, generally, the Cu(110) surface shows high stability within this bridge configuration on the Cu(110) surface (13). This was obvious with the deposition of terephthalate

monolayer (terephthalic acid) on Cu(110), where no significant effect of the terephthalate monolayer on the geometry of the copper surface atoms was observed, with only a small outward relaxation of the copper atoms on the first layer (13, 14, 16). This happened because copper atoms exhibit high coverage adsorption (13, 14, 16). In addition, they showed that the hydrogen atoms are shared between the carboxylate group of the neighbouring molecules to form Van der Waals crystalline solids (16).

In terms of the geometry of the adsorbed formate species, it was experimentally found that the formate is adsorbed on the copper surface *via* dehydrogenation (generally on a clean surface of copper) at elevated temperatures of 573–723 K (13). In addition, the formate species can be adsorbed *via* the release of water from the formic acid on an oxygen-pre-covered copper surface (13, 17). For high (two molecules in  $(2 \times 2)$  unit cell) and low formate coverage (one molecule in  $(2 \times 2)$  unit cell) on a Cu(110) surface, it was found that the most stable structure for high coverage is that in which both of the molecules are sitting in a bridge position, where the oxygen atom is bonded with one copper atom (13, 17). On the other hand, it was found that most stable configuration for low coverage is that with a bridge position with each oxygen atom bonded to a single copper atom on the  $[1\bar{1}0]$  plane (13). However, it was found that the Cu–O bond lengths are the same in all formate configurations (13, 16). In addition, the bond length of the oxygen atoms of the carboxylate group is the same even with the presence of oxygen adsorption in the first layer, but not the adsorption energy, which differs with any additional oxygen adsorption (15). Generally, attractive intermolecular interaction takes place between the adsorbed molecules of formate with high energy barriers against any additional presence of formate molecules on the formate-covered Cu(110) surface (15, 16). It was reported by Poulston *et al.* that the formate-adsorbed structure has higher mobility and become more oriented when the repulsive intermolecular interaction in the  $[001]$  direction is overcome, either with an oxygen-pre-covered Cu(110) surface or by increasing the formate coverage, as was shown *via* scanning electron microscopy (STM) (17). Furthermore, it was found that Cu(111) had the longest O–Cu bond length as compared to the Cu(110) and Cu(110) surfaces (11, 14).

To understand the unique relationship between the formate and formic acid, it is essential to

investigate the geometrical and electronic structure of formic acid, particularly the investigation of the energy barriers for the abstraction of protons from both the *trans*- and *cis*-forms of the formic acid with a hydrogen atom adsorbed on the Cu(110), Cu(111) and Cu(100) surfaces. It was found that the *trans*-form ( $E_{\text{ad}} = -0.193$  eV) of the formic acid is more stable than its *cis*-form ( $E_{\text{ad}} = -0.094$  eV) (11). The stability of the *trans*-formic acid is attributed to its favourable molecular geometry and electronic structure, which minimise energy and promote stability (11). The adsorption of formic acid on copper surfaces is predominantly physical adsorption, characterised by weak van der Waals forces. Physical adsorption implies a low enthalpy of adsorption, indicating that formic acid can dissociate easily on copper surfaces. This is because the interaction between formic acid and the copper surface does not significantly alter the electronic orbital patterns, allowing for easy dissociation (11). The weak van der Waals forces involved in physical adsorption facilitate the reversible adsorption and desorption of formic acid on copper surfaces. This dynamic process allows formic acid to interact with the copper surface without undergoing strong chemical bonding, enabling its conversion to formate or other intermediates involved in methanol synthesis (11). This unique relationship between formate and formic acid stems from the stability of the *trans*-formic acid, the low enthalpy of adsorption and the involvement of weak van der Waals forces. These factors facilitate the reversible adsorption and dissociation of formic acid on copper surfaces, enabling its participation in the methanol synthesis pathway.

Low-index copper has higher planar density of atoms but lower surface energy and because of this, it was found that the formate adsorption energy of Cu(110) planes has the highest adsorption energy (14) compared to Cu(100) and Cu(111), which is similar to experimental observations (14, 18, 19). This means that greater hydrogenation of CO<sub>2</sub> into methanol requires a large inter-surface cluster area in order to have a higher number of adsorption surface intermolecular reactions (14, 20). It was observed experimentally, using *in situ* X-ray photoelectron spectroscopy (XPS), that the methanol fully adsorbs over the Cu(110) surface at 300 K without any reaction and when dioxomethylene (H<sub>2</sub>COO) species are formed, they then decompose into formaldehyde and hydroxyl at low temperatures (18, 21). As seen from our discussion above, the adsorption of formate on copper surfaces has been extensively investigated

via infrared (IR) spectroscopy and inelastic neutron scattering (INS) spectroscopy, but much less so on zinc oxide surfaces, especially via INS, even though there are some studies on the interaction of methanol on zinc oxide (22). Jin and Wang provide a comprehensive investigation of methanol adsorption on three distinct zinc oxide surfaces: ZnO(10 $\bar{1}$ 0), O-ZnO(000 $\bar{1}$ ) and Zn-ZnO(0001) (23). They found that on the nonpolar ZnO(1010) surface, methanol exhibits partial dissociation, forming an ordered adlayer with coexisting methanol, methoxy and hydroxyl species. Molecular desorption of methanol dominates at elevated temperatures, while a minor fraction decomposes at defect sites to yield formaldehyde, hydrogen and carbon monoxide (22). Methanol adsorption on the polar O-ZnO(000 $\bar{1}$ ) surface leads to dissociative adsorption, producing methoxy and hydroxyl species. These methoxy species further decompose to formaldehyde, hydrogen and carbon monoxide upon annealing (23). The polar Zn-ZnO(0001) surface exhibits a unique adsorption behaviour, where methanol dissociation at step edges generates methoxy and hydroxyl species. These acid-base pairs at step edges exhibit remarkable catalytic activity and selectivity for methanol oxidation to formate and dihydrogen at 520 K. The reacted formate subsequently decomposes to carbon monoxide, CO<sub>2</sub> and water at higher temperatures (23).

The co-adsorption of formate species with hydrogen atoms on copper surfaces plays a crucial role in the methanol synthesis pathway, particularly on the low-index planes of Cu(110), Cu(100) and Cu(111). This co-adsorption facilitates the hydrogenation of formate to methanol. Studies have shown that hydrogen atoms preferentially co-adsorb on specific sites on these copper surfaces. On Cu(111), hydrogen atoms tend to co-adsorb on the threefold face-centred cubic sites, while on Cu(100), they favour the fourfold hexagonal close packed sites. However, on Cu(110), hydrogen atoms are most stable on the short bridge sites (11). The stability of hydrogen atoms on these specific sites is attributed to favourable interactions with the surrounding copper atoms, minimising the overall energy of the system. The application of different exchange-correlation functionals, such as PW91, PBE, PBEsol and PBE-D2, has confirmed that the Cu-H<sub>adsorbed</sub> bond distances are similar on all low-index copper surfaces (11). The formate pathway is considered the most suitable route for CO<sub>2</sub> hydrogenation to methanol compared to the reverse water-gas shift (RWGS)+CO-

hydrogenation pathway. This is because the formate pathway avoids the formation of strongly bound carbon monoxide intermediates, which can hinder the overall reaction progress. The weakness of carbon monoxide binding and the hindered hydrogenation to HCO species on copper surfaces make the RWGS+CO-Hydrogenation pathway less favourable (24). In contrast, the formate pathway proceeds through more energetically favourable intermediates, leading to efficient methanol synthesis. In summary, the co-adsorption of formate and hydrogen atoms on specific sites of copper surfaces facilitates the formate pathway for methanol synthesis. The stability of these co-adsorbed species and the avoidance of strongly bound carbon monoxide intermediates make the formate pathway more efficient than the RWGS+CO-hydrogenation pathway (11, 24).

## 2. Electronic Properties of Cu/ZnO Catalyst

Zinc oxide is a compound of zinc and oxygen that exists in a number of different crystalline forms. The electronic structure of zinc oxide is characterised by a valence band consisting of oxygen 2p orbitals and a conduction band consisting of zinc 4s and 4p orbitals. Zinc oxide exhibits interesting electronic properties including a direct bandgap of 3.3 eV, which is relatively large compared to other semiconductors. The valence band of zinc oxide is relatively flat, which gives it a high electron mobility and makes it a good conductor. The electronic properties of zinc oxide contribute to its catalytic activity. The wide bandgap of zinc oxide allows it to readily accept electrons, which makes it an effective reducing agent. The high electron mobility of zinc oxide also allows it to readily transport electrons to the surface, where they can participate in catalytic reactions. Zinc oxide has an electron mobility higher than  $>100 \text{ cm}^2 \text{ V}^{-1} \text{ s}^{-1}$  (25) and an excitation binding energy of 60 meV (26). These properties arise from the impurity-free crystal structure of zinc oxide crystals, which have few dislocations. **Table I** shows the obtained theoretical and experimental values of volume-per-formula units for zinc oxide in wurtzite, zinc blende and rocksalt structures.

The reaction conditions for CO<sub>2</sub> hydrogenation to methanol typically involve moderate pressures. However, some studies have explored the effects of high pressure on the properties of bulk zinc oxide. Jaffe *et al.* investigated the electronic properties of zinc oxide under high pressure and observed

**Table I The Theoretical and Experimental Results of Volume-Per-Formula Units for zinc oxide in Wurtzite, Zinc Blende and Rocksalt Structures (27–31)**

Structure type	Experimental results		Theoretical results		
	Ref. (27)	Ref. (28)	Ref. (29)	Ref. (30)	Ref. (31)
			LDA	GGA	HF
<b>Wurtzite, <math>V_0(\text{Å}^3)</math></b>	23.81	23.79	23.6	23.83	24.57
<b>Rocksalt, <math>V_0(\text{Å}^3)</math></b>	19.60	19.48	19.08	20.50	19.79
<b>Zinc blende, <math>V_0(\text{Å}^3)</math></b>	–	–	22.91	23.84	24.55

structural phase transformations to rocksalt and caesium chloride structures at a pressure of 9 GPa, accompanied by a 17% reduction in unit cell volume. This transformation is attributed to the soft elastic behaviour of zinc oxide and the increased ionicity of bonds under high pressure, favouring coulombic interactions over covalent bonding (31). At a much higher pressure of 260 GPa, zinc oxide undergoes another phase transition from the rocksalt structure to a cubic caesium chloride structure, with a 5% reduction in unit cell volume. This further emphasises the role of pressure in inducing structural changes in zinc oxide (27). The findings of Zaoui and Sekkal corroborate this pressure-induced phase transformation behaviour (32). They observed that the variation of bond ionicity decreases under high pressure, leading to stronger covalency and a rearrangement of atoms, ultimately resulting in phase transitions (32). These findings highlight the pressure-induced structural flexibility of zinc oxide. However, the pressures used in these studies are significantly higher than those employed in CO<sub>2</sub> hydrogenation reactions (tens of megapascals). Therefore, the direct applicability of these high-pressure phase transitions to reaction conditions needs careful consideration. Furthermore, Nause and Nemeth reported that the electron mobility of bulk zinc oxide grown *via* the pressurised melt method is approximately 298 cm<sup>2</sup> V<sup>-1</sup> s<sup>-1</sup> at 77 K, which is in reasonable agreement with Monte Carlo calculations that yielded an electron mobility of 74 cm<sup>2</sup> V<sup>-1</sup> s<sup>-1</sup> (33). However, the high electron mobility in the bulk zinc oxide might not directly translate to a significant impact on the catalytic performance of Cu/ZnO catalysts for CO<sub>2</sub> conversion. In these catalysts, the key reaction zones are located at the interface between copper and zinc oxide nanoparticles.

The first investigation of the electronic structure of Cu/ZnO was conducted by Herman *et al.* in 1979 using XPS-Auger (34). They found from X-ray fluorescence analysis that the copper in zinc oxide

shows two morphological crystalline phases of copper(II) oxide on zinc oxide, in which hexagonal structures of copper(II) oxide are present on the zinc oxide phase, which has network of six-fold rotation (34). They further observed that the adsorption edge of zinc oxide is located at 373 nm. Additionally, they found that d-hump energy shows that copper's electronic properties are independent of the presence of zinc oxide (34). Furthermore, they found that the d-hump energy in Cu/ZnO catalysts is low as compared to free copper, suggesting electron transfer from copper to the Cu/ZnO system (34). This electron transfer could potentially influence copper's catalytic activity. Moreover, they observed two planes: (i) the basal plane (~40–70% Cu/ZnO); (ii) the prism plane (~2–30% Cu/ZnO) and both had high surface area as well as high selectivity (34).

In terms of the Cu/ZnO catalyst function, the zinc oxide activates the hydrogen atom through heteropolar splitting, which leads to the formation of OH and ZnH groups on the zinc oxide surface (35). The bulk structure of zinc oxide is responsible for the poor chemisorption Cu/ZnO catalyst activity towards carbon monoxide (34, 35). However, this occurs due to the empty d-orbital of zinc 3d orbitals for back-donation (34). Moreover, the copper 3d orbitals electron configuration is responsible for the carbon monoxide binding by copper in the Cu/ZnO catalyst due to the size of unscreened copper 3d orbitals for back-bonding into the  $\pi$  orbitals of carbon monoxide (34). In terms of the electronic band structure of Cu/ZnO, Beltrán *et al.* calculated the band structure using the Hartree–Fock theory and DFT with the B3LYP hybrid exchange and correlation functional (36). They found that even though the two band structures of zinc oxide are topologically similar, they differed with respect to the direct band gaps of 12.0 eV and 3.20 eV based on the HF and B3LYP levels, respectively. They concluded that the B3LYP exchange and correlation functional gave a more accurate zinc oxide band structure, which was close to the experimental

data obtained by Wander and Harrison. In addition, using density of states, they reported that the zinc 3d orbitals are completely filled and localised at narrow bands of  $-4.0$  eV, while the zinc 4d orbitals are empty (36). On the other hand, they found that oxygen 2p orbitals are occupied, with a broad band between  $-4$  eV and  $0$  eV (36). Studies on the adsorption of copper atoms on zinc oxide have been also reported; for example, Beltrán *et al.* simulated the adsorption of copper atoms on zinc and oxygen ions on the zinc oxide surface. They estimated the binding energy at the HF level and they found that the adsorption energies of each model were  $253.5$  kJ mol<sup>-1</sup> and  $254.8$  kJ mol<sup>-1</sup>, respectively.

### 3. Bulk Structure of Cu/ZnO Catalyst

The hexagonal wurtzite zinc oxide structure is used in Cu/ZnO catalysts because it is more stable than its rocksalt and zinc blend structures. The wurtzite zinc oxide belongs to the P63mc space group, which consists of two merging hexagonal close-packing planes of zinc cations and oxygen anions along the c-axis (32). It has been reported that there is a linear dependence of methanol production rate on copper surface area, which means that the turnover frequency (TOF) is constant and independent of the composition without any influence of structural parameters on catalytic activity (37). Further to this, the TOF, as a function of zinc content, affects the methanol synthesis activity like the copper surface area (37, 38).

Looking more closely on the morphology of Cu/ZnO catalysts, transmission electron microscopy (TEM) characterisation shows that lattice defects in the copper lattice arise from planar defects, strain, twinning and fault defects which are clearly related to the activity of the catalyst (39). In addition, Kasatkin *et al.* reported that no correlation was observed between copper particle size as measured with TEM and catalytic activity, but it was obvious that the most active sites had the largest surface area and the least active had the smallest (39). In addition, they found that large copper particles contains more defects than the small particles (39). This was confirmed *via* kinetic Monte Carlo (kMC) simulation, which showed that the surface defects of Cu(111)/ZnO promote the highest catalytic activity for the hydrogenation of CO<sub>2</sub> to methanol as compared to the other copper/metal-oxide alloys (40). In general, zinc oxide can adsorb hydrogen at room temperature *via* two adsorption processes. In the first type, the hydrogen molecule may heterolytically dissociate to form two reactive species on the zinc oxide surface,

i.e., Zn-H and Zn-O-H, in a rapid and reversible manner (41). The second type of hydrogen adsorption is reversible, forming two bridged O-H-O and Zn-H-Zn species. In addition to the above adsorption processes, there can be a third type of adsorption, which was reported by Chang and Kokes (42). In the third type of hydrogen adsorption, a reversible process on zinc oxide may occur at low temperatures (77 K) and contain perturbed, non-dissociated hydrogen molecules (41–43). The studies by Tsyganenko *et al.* (44) as well as Hussain and Sheppard (43) successfully identified some of the stretching and bending modes of adsorbed hydrogen, providing valuable insights into the adsorption behaviour and surface interactions of hydrogen on Cu/ZnO catalysts. However, not all vibrational modes were detected, suggesting that further improvements in experimental techniques or theoretical modelling may be needed to fully characterise the vibrational spectrum of adsorbed hydrogen.

The bulk structure of Cu/ZnO catalysts plays a crucial role in their activity. While traditional characterisation techniques provide valuable information, INS offers unique insights due to its sensitivity to hydrogen and oxygen vibrations within the lattice (44, 41–43). Studies by Howard *et al.* (41) and Zhang *et al.* (45) employed INS to identify bending modes of Zn-O-H species. However, limitations in spectrometer sensitivity prevented observation of Zn-H or O-H stretching modes. Howard *et al.* further investigated the adsorption of hydrogen on zinc oxide using incoherent INS. They observed an intense broad band at  $1346$  cm<sup>-1</sup> for zinc oxide in the INS spectrum, which was the same as the intensity of the band in the INS spectrum for the adsorption of hydrogen on zinc oxide (Kadox 25). This mean that hydrogen shows strong dissociative adsorption on zinc oxide and carbonate impurities within the lattice in bulk zinc oxide provides the only way to raise that band (41, 42). Gogate *et al.* (46) proposed that oxygen vacancies within zinc oxide facilitate hydrogen atom spillover towards the Cu-ZnO interface. This spilled hydrogen can then participate in CO<sub>2</sub> hydrogenation to form formate species. These findings highlight the importance of bulk zinc oxide properties in influencing interfacial reactions on Cu/ZnO catalysts. Galván *et al.* (47) studied the relationship between copper content, catalyst activity and activation energy for the RWGS reaction (see **Figure 1**). They observed a trend of lower activity per catalyst mass (higher activation energy) with increasing copper content. This suggests that the presence of copper promotes the RWGS reaction at the Cu-ZnO interface.

#### 4. Influence of Cu/ZnO Catalyst Microstructure on Methanol Synthesis Activity

The microstructure of Cu/ZnO catalysts plays a crucial role in determining their catalytic activity for methanol synthesis from CO<sub>2</sub> and hydrogen. Several key microstructural features influence the adsorption, activation and conversion of reactants, ultimately affecting methanol production rates and selectivity (46, 48). The surface area of copper particles is a critical factor governing the availability of active sites for reactant adsorption and activation. A larger copper surface area provides more sites for CO<sub>2</sub> and hydrogen to interact with the catalyst, increasing the probability of reaction events and promoting methanol formation (13, 49–51). The morphology of zinc oxide particles can influence the dispersion of copper particles and the accessibility of active sites. Zinc oxide, with a high surface area and a porous structure, can provide a better support for copper particles, promoting uniform dispersion and maximising the exposure of active sites to reactants (50, 52–54). The size of copper particles affects the distribution of active sites and the diffusion of reactants and intermediates. Smaller copper particles generally exhibit higher catalytic activity due to their larger surface-to-volume ratio, providing more active sites per unit mass of catalyst. However, excessively small particles can hinder diffusion and limit the overall reaction rate (55–57). The microstructural strain in both copper and zinc oxide particles can affect their electronic properties and modify the adsorption strength of reactants. Moderate strain can optimise the d-band centre of copper, enhancing its ability to bind and activate CO<sub>2</sub> (58–60). Strain in zinc oxide can create defect sites that act as additional active sites and facilitate electron transfer. It was found that the main source of micro-strain is the fraction of the minority phase of zinc oxide that is dissolved in the bulk copper structure (58, 59). In addition, Günter *et al.* found that the residual oxygen in the copper matrix from the incomplete reduction of copper in zinc oxide is another origin of micro-strain in the Cu/ZnO microstructure (52). Furthermore, the variation in interfacial lattice strain that is caused by epitaxial bonding between copper and zinc oxide is another origin of micro-strain (61). The micro-strain in Cu/ZnO is responsible for the strong carbon monoxide band shift seen *via* Fourier transform infrared (FTIR) that indicates the formation of a zinc-copper surface alloy *via* the movement of zinc oxide moieties

into reduced copper micro-crystallites (38, 51). However, it was found that the formation of a zinc-copper alloy phase shows high activity in increasing the methanol production (52, 62).

Understanding the influence of zinc oxide crystal facets in Cu/ZnO catalysts is important because these faces directly interact with copper species at the interface, which significantly impacts the activity of CO<sub>2</sub> hydrogenation to methanol (58–60). This is primarily due to the interaction between the copper species and the zinc oxide support. Zinc oxide promotes the dispersion of copper nanoparticles on the catalyst surface. Additionally, zinc oxide acts as a reservoir for hydrogen and facilitates its spillover to the copper sites, where CO<sub>2</sub> hydrogenation occurs (58, 59). This spillover of hydrogen is crucial for the reaction. Studies by Lei *et al.* suggest that the specific crystallographic faces of zinc oxide in contact with copper can influence catalytic activity (60). They found that the (002) face of zinc oxide exhibits the highest activity for CO<sub>2</sub> hydrogenation to methanol. This is attributed to the (002) face having the highest polarity and containing the greatest concentration of oxygen vacancies. These oxygen vacancies are believed to play a role in the adsorption and activation of CO<sub>2</sub> molecules.

Hydrogen activation plays a crucial role in CO<sub>2</sub> conversion to methanol on Cu/ZnO catalysts *via* the hydrogen spillover mechanism. This mechanism involves physisorption and chemisorption of hydrogen in which hydrogen molecules first weakly adsorb (physisorb) onto the copper surface. Subsequently, they dissociate into hydrogen atoms, which become strongly bound (chemisorbed) to the copper surface through chemical bonds. Due to the close proximity of copper and zinc oxide in the catalyst structure, chemisorbed hydrogen atoms can migrate from the copper surface to the zinc oxide surface through a process called spillover. Once on the zinc oxide surface, the spilled-over hydrogen atoms react with adsorbed CO<sub>2</sub> to form formate species, which are key intermediates in methanol production. There are many factors influencing hydrogen spillover such as, metal-oxide interface which is the region that facilitates hydrogen diffusion between copper and zinc oxide. Another factor is metal loading where higher copper loading generally increases active site density, leading to more hydrogen atoms available for spillover and potentially enhancing catalyst activity. However, excessive copper loading can lead to detrimental effects like sintering and deactivation. Moreover, higher temperatures enhance hydrogen atom

mobility, potentially promoting spillover. However, excessively high temperatures can negatively impact catalyst performance (63–65).

Building upon the established high activity of Cu/ZnO catalysts for methanol synthesis compared to other systems (66–72), researchers have explored how tailoring the microstructure of these catalysts can further enhance their performance. Burch *et al.* found experimentally that the Cu/ZnO catalyst had the highest activity and efficiency compared to copper-support catalysts including gallium oxide, zirconia and alumina (70). Generally, the activity of the Cu/ZnO catalyst can be enhanced through the modification of the catalyst structure, using different family classes of additives or supports that promote the activity of the active centres (38, 60, 70). In addition, it was concluded by Günter *et al.* that a high copper surface area is required to activate the Cu/ZnO catalyst. This was observed from the high TOF of methanol synthesis through Cu/ZnO, with a positive correlation with micro-strain within copper crystallites (52). Moreover, Günter *et al.* observed that the expansion of the copper lattice increases the TOF of methanol through Cu/ZnO (52). In addition, the copper surface area promotes the synergistic interaction between copper and zinc oxide and because of this, the surface area of copper is a factor affecting the activity of Cu/ZnO catalysts (38, 61, 73).

In both the RWGS and formate pathways, additional phases play critical roles in enhancing the activity of the catalysts. For example, Schottky defects occurs in Cu–ZnO interfaces due to the oppositely charged ions of  $\text{Cu}^-$  and  $\text{Cu}^+$  that leave their lattices and create vacancies in the stoichiometric unit to maintain the overall charge of the interface. This leads to Schottky barriers at the Cu–ZnO interface that contributes to the activity of the catalyst. These formed Schottky barriers at the interface are promoted by electron transfer from the conduction band of zinc oxide into the copper, as revealed through XPS (55, 74, 75). It is worth mentioning that Liao *et al.* found that the interaction between copper nanoparticles and zinc oxide polar plates is significantly larger compared to copper nanoparticles and zinc oxide rods because they exhibit a higher number of polar faces and additionally, they found that that the Cu/ZnO plate system shows a higher selectivity for methanol compared to the Cu/ZnO rod systems, which means they emitted less carbon monoxide (74). Furthermore, the oxygen vacancies that form at the surface of zinc

oxide crystals are also active sites that contribute to selectivity for  $\text{CO}_2$  conversion into methanol (47). This strong electronic interaction between the copper and zinc oxide was demonstrated by various studies, such as temperature programmed reduction which shows that the reducibility of some oxygen atoms from zinc oxide increases with the presence of copper (74, 55). Numerous studies have consistently demonstrated that the generation of byproduct water during the RWGS reaction has a detrimental impact on the activity of Cu/ZnO catalysts (74, 55). This adverse effect stems from the adsorption of water molecules onto the catalyst surface, which effectively blocks the active sites responsible for  $\text{CO}_2$  activation and methanol synthesis. The presence of these adsorbed water molecules hinders the access of reactants to the active sites, thereby reducing the overall reaction rate and methanol production (48, 75–77).

## 5. Multiscale Modelling of Active Sites on the $\text{CO}_2$ Conversion to Methanol over Cu/ZnO-Based Catalyst

Recently, the kMC was employed in order to discriminate the active sites and mechanisms of the catalyst Cu/ZnO. In particular, meso-scale kMC simulation has been coupled with first principles calculations of DFT in order to find the catalytic surface coverage changes for the hydrogenation of  $\text{CO}_2$  into methanol through a Cu/ZnO/ $\text{Al}_2\text{O}_3$  catalyst. The kMC simulation output can help to identify the key intermediates from the statistical simulation of each reaction step at specific, defined reaction conditions. Pavlišič *et al.* employed kMC simulation with the same industrial operating conditions of methanol synthesis, with a temperature of 500 K and a pressure of 40 bar (78). They found that the richest surface species intermediates are active site of H, HCOO and  $\text{CH}_3\text{O}$  intermediates. This means that those species have a prohibitively high activation energy and it proves that methanol is produced on the formate pathway through HCOO,  $\text{H}_2\text{CO}$ ,  $\text{H}_2\text{COOH}$  and  $\text{H}_2\text{CO}$  (78).

Looking more closely at the surface chemical kinetics through kMC simulations, Yang *et al.* investigated the formate and RWGS+CO-hydrogenation pathways through copper catalysts with different doping (gold, platinum and gold-rhodium) through kMC to identify the best choice of reaction pathway for methanol production with each doping (79). They found that with and without doping with all of the studied elements,

the formate pathway dominates the reaction and they also found that doping strongly increases the overall methanol production. In addition, they found that the RWGS pathway is faster than the formate pathway in accelerating the conversion of carbon monoxide into methanol through copper-based catalysts. This supports our approach to the role of the copper in stabilise the surface-adsorbed particles such as HCO and carbon monoxide and the importance of doping in accelerating the conversion of CO<sub>2</sub> into methanol.

Considering the role of the zinc oxide surface in methanol synthesis, an accelerated *ab initio* molecular dynamics (AIMD) approach has also been developed by Kiss *et al.* to investigate the free energy landscape of the reaction pathway of carbon monoxide conversion into methanol. They found, from the obtained free energy landscape simulations, that formaldehyde H<sub>2</sub>CO species (formate pathway) during hydrogenation have two different charge states, which are F<sup>0</sup> and F<sup>-</sup> defect sites where the F<sup>-</sup> is created *via* the desorption of hydrogen from oxygen atoms in the vicinity of oxygen defect sites (80). This observation means that the decomposition of dioxomethylene (H<sub>2</sub>COO) into formaldehydes depends on the reduction state of formaldehyde (81). Another approach was conducted by Hegemann *et al.*, who employed the *ab initio* method to investigate the adsorption of copper on polar ZnO (0001) and ZnO(000 $\bar{1}$ ) in order to investigate the active sites of Cu/ZnO/Al<sub>2</sub>O<sub>3</sub> (49). They found that charger transfer occurs from copper to zinc at the short binding surface, which was weak charge transfer. However, the long surface distance Cu–ZnO interaction is dominated by polarisation as the copper atom is polarised by the zinc oxide, which therefore increases the dipole moment of the system. However, the critical finding is that they proved that copper is able to stabilise the polar zinc oxide surfaces *via* a charge transfer mechanism. However, they indicated that the copper bonds to the zinc oxide surfaces are weaker than the hydrogen and hydroxyl bonds (49, 82, 83). This means that copper atoms induced the formation of oxygen vacancies in zinc oxide, which proves that the zinc oxide acts as the active site and therefore a storage for hydrogen atoms, while the methanol formation take place on the copper particles (49, 84).

In terms of the complex interfacial on Cu/ZnO catalysts with a promoter, Yang *et al.* employed kMC simulation in order to investigate the Cu(111)/ZnO and pure copper model systems

during the CO<sub>2</sub> hydrogenation into methanol (8). They identified HCOO as the spectator of the reaction and the key active intermediate in the copper catalyst system. In addition, they found that the addition of zinc oxide or zinc to Cu/ZnO increases the stabilisation of HCOOH intermediate species during the hydrogenation of CO<sub>2</sub> through the activation of HCOO (24). It is obvious from the reported kMC simulation results that the higher loading of copper causes a higher dispersion of copper, leading to higher activity of the Cu/ZnO catalyst. This means that the larger metallic exposed copper surface with the promoter zinc oxide will directly increase the activity of the active phase on the catalyst. In addition, they concluded that the large dispersion of zinc sites on the copper surface leads to higher methanol production (85). This simulation supported the findings of Kattel *et al.*, who found that the deposition of small particles of copper on the surface of clean zinc oxide will causes higher activity in the system for methanol synthesis because the small copper particle have a higher concentration of the edge of atoms (24). Furthermore, microkinetic modelling indicates that copper is the active phase which promotes zinc oxide, causing synergy interfacial interactions that promote methanol production (86–89).

One of the early investigations of the geometry of active sites was conducted by French *et al.*, who used the hybrid quantum mechanics/molecular mechanics (QM/MM) approach to define the chemisorption of methanol intermediate species on the polar ZnO(001). They found that the formation of anionic adsorbates occurs on the oxygen interstitial surface site. This atomistic model of the active site has the ability to trap the electron so that adsorption takes place and can accommodate (O<sup>1-</sup>) oxygen anions (90). In addition, they found that this site is able to trap an electron; therefore, adsorption can occur by forming a surface anionic species and transfer of an electron to the neutral active site occurs with the adsorption of neutral adsorbates. From the above discussion, it is obvious that the experimental result is consistent with the computational simulation result, which shows that Cu/ZnO catalysts with copper and zinc oxide form highly active sites that lead to extremely high methanol selectivity.

## 6. Modifications of Cu/ZnO Catalyst

The intricate relationship between surface structure and catalytic performance drives the

development of enhanced Cu/ZnO catalysts for CO<sub>2</sub> hydrogenation to methanol. By modifying copper active sites, researchers aim to increase the dispersion of the active phase, promoting interactions between the catalyst and CO<sub>2</sub> and boosting CO<sub>2</sub> conversion (60, 91). A pioneering approach involves incorporating zirconia, a tetravalent metal oxide with weak hydrophilicity, into the catalyst structure. Zirconia enhances copper stability and dispersion, maximising the availability of active sites for CO<sub>2</sub> adsorption and activation (53, 92). Furthermore, doping Cu/ZnO with zirconia elevates the catalyst's basicity (93), favouring CO<sub>2</sub> adsorption and enhancing selectivity towards methanol formation (94). Microstructure imaging reveals the formation of oxygen vacancies during CO<sub>2</sub> reduction, further substantiating the role of zirconia in promoting high copper dispersion and catalytic activity (71, 95). According to the reaction network proposed by Arena *et al.*, the remarkable promotion effect of zirconia stems from the Cu–ZnO interface (see Figure 1 in Part I (1)). Here, the reduction of Zr<sup>3+</sup> ions facilitate the binding of crucial reaction intermediates, such as formaldehyde and aldehyde (94). Additionally, Cu<sup>δ+</sup> sites, stabilised by interactions with zinc oxide and zirconia surface sites, play a pivotal role in the formation and hydrogenation of these intermediates (94, 96). In essence, incorporating zirconia into Cu/ZnO catalysts enhances catalytic performance by increasing copper dispersion, promoting CO<sub>2</sub> adsorption and stabilising active Cu<sup>δ+</sup> sites. These modifications lead to improved CO<sub>2</sub> conversion and methanol selectivity, establishing Cu/ZnO/ZrO<sub>2</sub> catalysts as promising candidates for efficient methanol synthesis from CO<sub>2</sub> hydrogenation (94).

Another example of a mesoporous material that is used as modifier of Cu/ZnO is gallium oxide, which can easily generate Cu–ZnO nanoparticles due to the existence of Ga<sup>3+</sup> within the Cu/ZnO catalyst that can moderate the thermal reduction of zinc oxide. In addition, it was found that the increases in Zn<sup>0</sup> species with copper particles at the interface can enhance the performance of CO<sub>2</sub> hydrogenation into methanol by increasing the adsorption strength of surface intermediates (93). Similarly, the formation of staggered gap heterojunctions can increase the adsorption strength of surface intermediates, leading to faster hydrogenation CO<sub>2</sub> into methanol, like the electronic heterojunction between the gallium spin (ZnGa<sub>2</sub>O<sub>4</sub>) with gallium oxide (10, 97, 98). Furthermore, Li *et al.* found that the formation of hydrotalcite precursors during

the synthesis of hydroxycarbonate precursors improves the copper dispersion and the formation of Cu–ZnO sites on Cu/ZnO/Ga<sub>2</sub>O<sub>3</sub> (50, 99).

Recent studies have found that carbonaceous material can also improve the performance of Cu/ZnO catalysts in terms of adsorption strength and surface availability for formate by using them as a modifier/support, such as carbon copper–zinc/graphene aerogel catalysts (100), multiwalled carbon nanotubes (MWCNTs) (101) and copper–zinc-polymeric materials (BTC) (93, 102). The mixing of those surface sites can improve the adsorption/activation of hydrogen and CO<sub>2</sub> in Cu/ZnO-based catalysts due to the formation of highly active formate intermediates through CO<sub>2</sub> adsorption. In terms of MWCNTs, it was found that the presence of nanotubes as spacers between copper and zinc oxide particles can improve copper dispersion and for CO<sub>2</sub>, that leads to higher selectivity into methanol. This occurs because of the synergy effect of Cu–ZnO with CNTs due to the presence of Zn<sup>+</sup> at the stepped copper surface as both particles of Cu/ZnO are supported on wells (101). Moreover, graphene oxide aerogel was commonly used as a supporter for Cu/ZnO catalysts for methanol as it provides a high surface area for CO<sub>2</sub> hydrogenation. Furthermore, bimetallic CuZn-BTC can also be employed as supporter to generate multi-interfacial sites of Cu–ZnO and prevent the accumulation of copper and zinc oxide nanoparticles, which enhances the performance of CO<sub>2</sub> hydrogenation into methanol.

Angelo *et al.* conducted a comprehensive investigation into the influence of modifying Cu/ZnO-based catalysts with zirconia, ceria and alumina on CO<sub>2</sub> conversion and methanol synthesis under conditions of 553 K and 5 MPa pressure (88). Their findings revealed that zirconia emerged as the most effective modifier for enhancing both CO<sub>2</sub> conversion and methanol productivity compared to alumina and ceria (76, 79, 88). In terms of CO<sub>2</sub> conversion, Cu/ZnO/ZrO<sub>2</sub> again exhibits the highest CO<sub>2</sub> conversion with 23.2%, followed by Cu/ZnO/Al<sub>2</sub>O<sub>3</sub> (19.5%) and Cu/ZnO/CeO<sub>2</sub> (12.8%). In terms of methanol productivity, zirconia-modified catalysts demonstrated superior performance, achieving a remarkable methanol productivity of 331 g<sub>MeOH</sub> kg<sub>cata</sub><sup>-1</sup> h<sup>-1</sup> at 553 K (88). This finding aligns with the results reported by Arena *et al.*, who observed that Cu/ZnO/ZrO<sub>2</sub> catalysts exhibited the highest methanol productivity of 65 g<sub>MeOH</sub> kg<sub>cata</sub><sup>-1</sup> h<sup>-1</sup> at 473 K and 1.0 MPa (94). Furthermore, Bonura *et al.* proposed a novel preparation method for Cu/ZnO/ZrO<sub>2</sub> catalysts,

leading to an enhanced methanol productivity of  $305 \text{ g}_{\text{MeOH}} \text{ kg}_{\text{cata}}^{-1} \text{ h}^{-1}$  at 513 K and 1 MPa pressure (95). This enhancement is attributed to the weak hydrophilicity of zirconia compared to alumina and ceria, which promotes copper dispersion and catalyst stability by hindering water absorption (79). Collectively, these studies underscore the effectiveness of zirconia as a modifier for Cu/ZnO-based catalysts in promoting CO<sub>2</sub> conversion and methanol synthesis. The superior performance of zirconia-modified catalysts stems from their enhanced copper dispersion and improved catalyst stability, making them promising candidates for efficient methanol production from CO<sub>2</sub> hydrogenation.

This work continues in Part III (103).

## Author Contributions

M.A.S.: formal analysis, data curation, writing original draft, software, methodology and validation.

## Conflicts of Interest

Author declares no conflict of interest.

## References

1. M. Al Salmi, *Johnson Matthey Technol. Rev.*, 2024, **68**, (4), 465
2. F. H. P. M. Habraken, G. A. Bootsma, P. Hofmann, S. Hachicha, A. M. Bradshaw, *Surf. Sci.*, 1979, **88**, (2–3), 285
3. R. A. Bennett, S. Poulston, M. Bowker, *J. Chem. Phys.*, 1998, **108**, (16), 6916
4. J. A. Rodriguez, S. D. Senanayake, D. Stacchiola, P. Liu, J. Hrbek, *Acc. Chem. Res.*, 2014, **47**, (3), 773
5. Y. Li, S. H. Chan, Q. Sun, *Nanoscale*, 2015, **7**, (19), 8663
6. S. Günther, L. Zhou, R. Imbihl, M. Hävecker, A. Knop-Gericke, E. Kleimenov, R. Schlögl, 'In situ X-ray Photoelectron Spectroscopy of the Methanol Oxidation Over Cu(110)', 2005: [https://pure.mpg.de/rest/items/item\\_739113/component/file\\_739112/content](https://pure.mpg.de/rest/items/item_739113/component/file_739112/content) (Accessed on 14th September 2023)
7. A. A. Khassin, V. V. Pelipenko, T. P. Minyukova, V. I. Zaikovskii, D. I. Kochubey, T. M. Yurieva, *Catal. Today*, 2006, **112**, (1–4), 143
8. Y. Yang, J. Evans, J. A. Rodriguez, M. G. White, P. Liu, *Phys. Chem. Chem. Phys.*, 2010, **12**, (33), 9909
9. L. C. Grabow, M. Mavrikakis, *ACS Catal.*, 2011, **1**, (4), 365
10. M. Behrens, F. Studt, I. Kasatkin, S. Kühl, M. Hävecker, F. Abild-Pedersen, S. Zander, F. Girgsdies, P. Kurr, B.-L. Kniep, M. Tovar, R. W. Fischer, J. K. Nørskov, R. Schlögl, *Science*, 2012, **336**, (6083), 893
11. A. Chutia, I. P. Silverwood, M. R. Farrow, D. O. Scanlon, P. P. Wells, M. Bowker, S. F. Parker, C. R. A. Catlow, *Surf. Sci.*, 2016, **653**, 45
12. M. D. Porosoff, B. Yan, J. G. Chen, *Energy Environ. Sci.*, 2016, **9**, (1), 62
13. N. Atodiresei, K. Schroeder, S. Blügel, *Phys. Rev. B*, 2007, **75**, (11), 115407
14. Z. Hu, R. J. Boyd, *J. Chem. Phys.*, 2000, **112**, 9562
15. J. R. B. Gomes, J. A. N. F. Gomes, *Surf. Sci.*, 1999, **432**, (3), 279
16. N. Atodiresei, V. Caciuc, K. Schroeder, S. Blügel, *Phys. Rev. B*, 2007, **76**, (11), 115433
17. S. Poulston, R. A. Bennett, A. H. Jones, M. Bowker, *Phys. Rev. B*, 1997, **55**, (19), 12888
18. Z.-M. Hu, K. Takahashi, H. Nakatsuji, *Surf. Sci.*, 1999, **442**, (1), 90
19. J. P. P. Ramalho, J. R. B. Gomes, F. Illas, *RSC Adv.*, 2013, **3**, (32), 13085
20. C. W. Bauschlicher, *J. Chem. Phys.*, 1994, **101**, (4), 3250
21. J. R. B. Gomes, J. A. N. F. Gomes, *Surf. Sci.*, 2001, **471**, (1–3), 59
22. G. J. Millar, C. H. Rochester, K. C. Waugh, *J. Chem. Soc. Faraday Trans.*, 1992, **88**, (15), 2257
23. L. Jin, Y. Wang, *Phys. Chem. Chem. Phys.*, 2017, **19**, (20), 12992
24. S. Kattel, P. J. Ramírez, J. G. Chen, J. A. Rodriguez, P. Liu, *Science*, 2017, **355**, (6331), 1296
25. E. M. Kaidashev, M. Lorenz, H. von Wenckstern, A. Rahm, H.-C. Semmelhack, K.-H. Han, G. Benndorf, C. Bundesmann, H. Hochmuth, M. Grundmann, *Appl. Phys. Lett.*, 2003, **82**, (22), 3901
26. B. P. Zhang, N. T. Binh, Y. Segawa, K. Wakatsuki, N. Usami, *Appl. Phys. Lett.*, 2003, **83**, (8), 1635
27. S. Desgreniers, *Phys. Rev. B*, 1998, **58**, (21), 14102
28. H. Karzel, W. Potzel, M. Köfferlein, W. Schiessl, M. Steiner, U. Hiller, G. M. Kalvius, D. W. Mitchell, T. P. Das, P. Blaha, K. Schwarz, M. P. Pasternak, *Phys. Rev. B*, 1996, **53**, (17), 11425
29. R. Ahuja, L. Fast, O. Eriksson, J. M. Wills, B. Johansson, *J. Appl. Phys.*, 1998, **83**, (12), 8065
30. J. E. Jaffe, A. C. Hess, *Phys. Rev. B*, 1993, **48**, (11), 7903
31. J. E. Jaffe, J. A. Snyder, Z. Lin, A. C. Hess, *Phys. Rev. B*, 2000, **62**, (3), 1660
32. A. Zaoui, W. Sekkal, *Phys. Rev. B*, 2002, **66**, (17),

- 174106
33. J. Nause, B. Nemeth, *Semicond. Sci. Technol.*, 2005, **20**, (4), S45
34. R. G. Herman, K. Klier, G. W. Simmons, B. P. Finn, J. B. Bulko, T. P. Kobylinski, *J. Catal.*, 1979, **56**, (3), 407
35. R. P. Eischens, W. A. Pliskin, M. J. D. Low, *J. Catal.*, 1962, **1**, (2), 180
36. A. Beltrán, J. Andrés, M. Calatayud, J. B. L. Martins, *Chem. Phys. Lett.*, 2001, **338**, (4–6), 224
37. T. Shishido, Y. Yamamoto, H. Morioka, K. Takaki, K. Takehira, *Appl. Catal. A: Gen.*, 2004, **263**, (2), 249
38. R. Burch, S. E. Golunski, M. S. Spencer, *J. Chem. Soc. Faraday Trans.*, 1990, **86**, (15), 2683
39. I. Kasatkin, P. Kurr, B. Kniep, A. Trunschke, R. Schlögl, *Angew. Chem. Int. Ed.*, 2007, **46**, (38), 7324
40. D. Kopač, B. Likozar, M. Huš, *Appl. Surf. Sci.*, 2019, **497**, 143783
41. J. Howard, I. J. Braid, J. Tomkinson, *J. Chem. Soc. Faraday Trans. 1 Phys. Chem. Condens. Phases*, 1984, **80**, (1), 225
42. C. C. Chang, R. J. Kokes, *J. Am. Chem. Soc.*, 1971, **93**, (25), 7107
43. G. Hussain, N. Sheppard, *J. Chem. Soc. Faraday Trans.*, 1990, **86**, (9), 1615
44. A. A. Tsyganenko, J. Lamotte, J. Saussey, J. C. Lavalley, *J. Chem. Soc. Faraday Trans. 1 Phys. Chem. Condens. Phases*, 1989, **85**, (8), 2397
45. L. Zhang, X. Zhang, K. Qian, Z. Li, Y. Cheng, L. L. Daemen, Z. Wu, W. Huang, *J. Energy Chem.*, 2020, **50**, 351
46. M. R. Gogate, *Pet. Sci. Technol.*, 2019, **37**, (5), 603
47. C. Álvarez Galván, J. Schumann, M. Behrens, J. L. G. Fierro, R. Schlögl, E. Frei, *Appl. Catal. B: Environ.*, 2016, **195**, 104
48. S. Kühn, A. Tarasov, S. Zander, I. Kasatkin, M. Behrens, *Chem. Eur. J.*, 2014, **20**, (13), 3782
49. I. Hegemann, A. Schwaebe, K. Fink, *J. Comput. Chem.*, 2008, **29**, (13), 2302
50. M. M.-J. Li, Z. Zeng, F. Liao, X. Hong, S. C. E. Tsang, *J. Catal.*, 2016, **343**, 157
51. E. Kampshoff, E. Hahn, K. Kern, *Phys. Rev. Lett.*, 1994, **73**, (5), 704
52. M. M. Günter, T. Ressler, B. Bems, C. Büscher, T. Genger, O. Hinrichsen, M. Muhler, R. Schlögl, *Catal. Lett.*, 2001, **71**, 37
53. X. Dong, F. Li, N. Zhao, F. Xiao, J. Wang, Y. Tan, *Appl. Catal. B: Environ.*, 2016, **191**, 8
54. D. Waller, D. Stirling, F. S. Stone, M. S. Spencer, *Faraday Discuss. Chem. Soc.*, 1989, **87**, 107
55. F. C. Meunier, *Angew. Chem. Int. Ed.*, 2011, **50**, (18), 4053
56. B. V. Farahani, F. H. Rajabi, M. Bahmani, M. Ghelichkhani, S. Sahebdehfar, *Appl. Catal. A: Gen.*, 2014, **482**, 237
57. A. Karelovic, P. Ruiz, *Catal. Sci. Technol.*, 2015, **5**, (2), 869
58. V. D. B. C. Dasireddy, N. S. Štefančič, B. Likozar, *J. CO<sub>2</sub> Util.*, 2018, **28**, 189
59. I. U. Din, M. S. Shaharun, M. A. Alotaibi, A. I. Alharthi, A. Naeem, *J. CO<sub>2</sub> Util.*, 2019, **34**, 20
60. H. Lei, R. Nie, G. Wu, Z. Hou, *Fuel*, 2015, **154**, 161
61. A. Urakawa, A. Bansode, R. V. Gaikwad, 'Methanol Production Process', *World Patent Appl.* 2017/140800, 24th August, 2017
62. T. Fujitani, J. Nakamura, *Catal. Lett.*, 1998, **56**, 119
63. M. Al Salmi, *Johnson Matthey Technol. Rev.*, 2024, **68**, (2), 184
64. K. Mori, N. Hashimoto, N. Kamiuchi, H. Yoshida, H. Kobayashi, H. Yamashita, *Nat. Commun.*, 2021, **12**, (1), 3884
65. R. Prins, *Chem. Rev.*, 2012, **112**, (5), 2714
66. M. Spencer, *Top. Catal.*, 1999, **8**, 259
67. J. Wang, S. Funk, U. Burghaus, *Catal. Lett.*, 2005, **103**, (3–4), 219
68. S. Fujita, M. Usui, H. Ito, N. Takezawa, *J. Catal.*, 1995, **157**, (2), 403
69. G. J. J. Bartley, R. Burch, *Appl. Catal.*, 1988, **43**, (1), 141
70. R. Burch, R. J. Chappell, S. E. Golunski, *Catal. Lett.*, 1988, **1**, (12), 439
71. C. Yang, Z. Ma, N. Zhao, W. Wei, T. Hu, Y. Sun, *Catal. Today*, 2006, **115**, (1–4), 222
72. C. Baltes, S. Vukojević, F. Schüth, *J. Catal.*, 2008, **258**, (2), 334
73. G. C. Chinchén, P. J. Denny, D. G. Parker, M. S. Spencer, D. A. Whan, *Appl. Catal.*, 1987, **30**, (2), 333
74. F. Liao, Y. Huang, J. Ge, W. Zheng, K. Tedsree, P. Collier, X. Hong, S. C. Tsang, *Angew. Chem. Int. Ed.*, 2011, **50**, (9), 2162
75. D. S. King, R. M. Nix, *J. Catal.*, 1996, **160**, (1), 76
76. C. D. Wagner, L. H. Gale, R. H. Raymond, *Anal. Chem.*, 1979, **51**, (4), 466
77. J. S. Lee, K. H. Lee, S. Y. Lee, Y. G. Kim, *J. Catal.*, 1993, **144**, (2), 414
78. A. Pavlišič, M. Huš, A. Prašnikar, B. Likozar, *J. Clean. Prod.*, 2020, **275**, 122958
79. Y. Yang, 'Rational Design of Cu-Based Nanocatalysts for the Production of Methanol', PhD Thesis, Stony Brook University, Stony Brook, NY, USA, 2013
80. J. Kiss, J. Frenzel, N. N. Nair, B. Meyer, D. Marx, *J. Chem. Phys.*, 2011, **134**, (6), 064710
81. P. Sharma, J. Sebastian, S. Ghosh, D. Creaser, L. Olsson, *Catal. Sci. Technol.*, 2021, **11**, (5), 1665

82. S. Poto, D. V. van Berkel, F. Gallucci, M. F. N. d'Angelo, *Chem. Eng. J.*, 2022, **435**, (2), 134946
83. P. Ren, W. Tu, C. Wang, S. Cheng, W. Liu, Z. Zhang, Y. Tian, Y.-F. Han, *Appl. Catal. B: Environ.*, 2022, **305**, 121016
84. J. C. Frost, *Nature*, 1988, **334**, (6183), 577
85. D. Kopač, B. Likozar, M. Huš, *ACS Catal.*, 2020, **10**, (7), 4092
86. J. Qaderi, *Int. J. Innov. Res. Sci. Stud.*, 2020, **3**, (2), 33
87. A. J. Medford, J. Sehested, J. Rossmeisl, I. Chorkendorff, F. Studt, J. K. Nørskov, P. G. Moses, *J. Catal.*, 2014, **309**, 397
88. L. Angelo, K. Kobl, L. M. M. Tejada, Y. Zimmermann, K. Parkhomenko, A.-C. Roger, *Comptes Rendus Chim.*, 2015, **18**, (3), 250
89. H. Bai, M. Ma, B. Bai, J. Zuo, H. Cao, L. Zhang, Q.-F. Zhang, V. A. Vinokurov, W. Huang, *J. Catal.*, 2019, **380**, 68
90. S. A. French, S. T. Bromley, A. A. Sokol, C. R. A. Catlow, J. Kendrick, S. Rogers, P. Sherwood, *MRS Proc.*, 2001, **677**, 93
91. K. Klier, *Adv. Catal.*, 1982, **31**, 243
92. C. Tisseraud, C. Comminges, T. Belin, H. Ahouari, A. Soualah, Y. Pouilloux, A. Le Valant, *J. Catal.*, 2015, **330**, 533
93. R. Guil-López, N. Mota, J. Llorente, E. Millán, B. Pawelec, J. L. G. Fierro, R. M. Navarro, *Materials*, 2019, **12**, (23), 3902
94. F. Arena, G. Mezzatesta, G. Zafarana, G. Trunfio, F. Frusteri, L. Spadaro, *J. Catal.*, 2013, **300**, 141
95. G. Bonura, M. Cordaro, C. Cannilla, F. Arena, F. Frusteri, *Appl. Catal. B: Environ.*, 2014, **152–153**, 152
96. S. Kattel, B. Yan, Y. Yang, J. G. Chen, P. Liu, *J. Am. Chem. Soc.*, 2016, **138**, (38), 12440
97. L. Qi, J. Li, *J. Catal.*, 2012, **295**, 59
98. T. Kamsuwan, A. Guntida, P. Praserttham, B. Jongsomjit, *ACS Omega*, 2022, **7**, (29), 25783
99. M. M.-J. Li, C. Chen, T. Ayvali, H. Suo, J. Zheng, I. F. Teixeira, L. Ye, H. Zou, D. O'Hare, S. C. E. Tsang, *ACS Catal.*, 2018, **8**, (5), 4390
100. V. Deerattrakul, P. Puengampholsrisook, W. Limphirat, P. Kongkachuichay, *Catal. Today*, 2018, **314**, 154
101. B. Zhang, Y. Chen, J. Li, E. Pippel, H. Yang, Z. Gao, Y. Qin, *ACS Catal.*, 2015, **5**, (9), 5567
102. C. Zhang, P. Liao, H. Wang, J. Sun, P. Gao, *Mater. Chem. Phys.*, 2018, **215**, 211
103. M. Al Salmi, *Johnson Matthey Technol. Rev.*, 2024, **68**, (4), 490

## The Author



Mustafa Al Salmi is a Production Engineer at Petroleum Development Oman (PDO). He received his BEng Chemical and Material Engineering from University of Leeds, UK, in 2021. He then completed his MSc Chemistry by Research from University of Lincoln, UK, and ISIS Neutron and Muon Source at the STFC Rutherford Appleton Laboratory near Oxford, UK between 2021 and 2023. His research expertise includes neutron vibrational spectroscopy techniques, first-principles computational modelling and data science to optimise chemical processes within the oil and gas industry. He also applies this knowledge to understand and predict heterogeneous catalysts and materials for use in sustainable chemical production, energy storage and pollution reduction. Additionally, his research background includes experience with various optimisation methods like differential evolution, particle swarm optimisation and simulated annealing, which he has employed to improve efficiency and performance in chemical engineering processes.